ACS OMEGA

http://pubs.acs.org/journal/acsodf

Article

Study on the Performance of the Zr-Modified Cu-SSZ-13 Catalyst for Low-Temperature NH_3-SCR

Huiyong Du, Shuo Yang,* Ke Li, Qian Shen, Min Li, Xuetao Wang, and Chenyang Fan

Cite This: *ACS Omega* 2022, 7, 45144−45152

Read Online

ACCESS | Metrics & More | Article Recommendations

ABSTRACT: Cu-SSZ-13 and Zr-modified Cu-SSZ-13 catalysts with different Zr/Cu mass ratios were prepared by ion-exchange and impregnation methods, respectively. The NH_3-SCR performance tests were performed using the catalyst performance evaluation device to investigate the effects of different Zr/Cu mass ratios on the catalyst ammonia-selective catalytic reduction (NH_3-SCR) performance. X-ray diffraction, ICP-OES, BET, NH_3 temperature-programed desorption (NH_3-TPD), H_2 temperature-programmed reduction (H_2-TPR), X-ray photoelectron spectrometry, and in situ diffuse reflectance infrared Fourier transform spectroscopy (in situ DRIFTS) were used to characterize the catalysts. The results show that the prepared Cu-SSZ-13 catalyst had good catalytic activity. Zr introduction was carried out on this basis. The results showed that proper Zr doping improved the catalytic activity at low temperatures and widened the high-temperature stage, with an optimal activity stage at a Zr/Cu mass ratio of 0.2. The NO_x conversion efficiency was close to 100% at 200 °C and over 80% at 450 °C. The active species were well dispersed on the catalyst surface, and the metal modification did not change the crystal structure of the zeolite. The NH_3-TPD results showed that the Zr-modified catalyst had more abundant acid sites, and the H_2-TPR results indicated that the Cu species on the catalyst had excellent reducibility at low temperatures. The interaction between Cu and Zr could regulate the Cu^+ and Cu^{2+} proportion on the catalyst surface, which facilitated the increase in the Cu^+ for fast SCR reaction at low temperatures. With abundant acid sites and both SCR reactions following the Eley−Rideal (E−R) and Langmuir−Hinshelwood (L−H) mechanism on the catalyst surface at a low temperature of 150 °C, more abundant acid sites and reaction paths created favorable conditions for NH_3-SCR reactions at low temperatures.

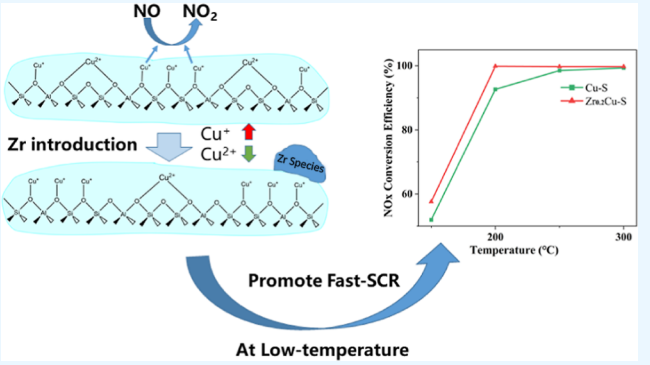

1. INTRODUCTION

With the increasingly stringent emission requirements of vehicles, the diesel particulate filter (DPF) system was used to remove the particulate matter to meet the regulations. Due to the characteristics of vanadium-based SCR catalysts, the high-temperature durability was terrible. Evaporation of vanadium metal and catalyst deactivation existed above 550 °C, which was a great hazard to the environment and human health. In light of this, V-based catalysts were not suitable for current diesel after-treatment systems. SSZ-13 molecular sieve had a chabazite (CHA) structure with a pore structure of 0.38 nm × 0.38 nm. Its excellent hydrothermal aging resistance and high specific surface area were crucial for NH_3-SCR.[1−4] Cu-SSZ-13 molecular sieve catalysts with transition-metal Cu as the active component had been widely used in lean combustion diesel engines and commercial vehicle after-treatment systems.[5] The Cu-based zeolite catalysts performed well in hydrothermal resistance and de-NO_x at low temperatures.[6,7] Besides, the Cu-SSZ-13 catalyst could also avoid irreversible deactivation and vanadium metal evaporation in the case of DPF regeneration.

In addition to single metal Cu-SSZ-13 catalysts loaded with Cu, researchers further enhanced the performance of Cu-SSZ-13 catalysts by doping with other metals. Fe-based catalysts had excellent NH_3-SCR performance at high temperatures.[8,9] Using different preparation and doping methods, iron and copper active components could co-exist in the composite catalyst. Due to the strong interaction between Fe and Cu species, Fe−Cu/SSZ-13 composite catalysts could widen the SCR reaction temperature range and improve the NH_3-SCR activity compared to Cu-SSZ-13 catalysts.[3,10,11] Ce doping could also improve the performance of Cu-SSZ-13 catalysts, and the appropriate amount of Ce doping could stabilize the zeolite structure and Cu active center to improve the

Received: August 30, 2022
Accepted: November 21, 2022
Published: November 29, 2022

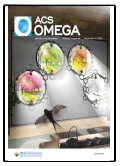

hydrothermal stability of the catalysts.[12,13] H_2 temperature-programmed reduction (H_2-TPR) experiments and in situ IR results showed that the doping of Ce could improve the redox performance of the catalysts. The synergistic utility between Cu and Ce species could enhance the surface adsorption of NH_3 and NO[14] to improve the NH_3-SCR performance of the catalyst. Other metal doping-modified Cu-SSZ-13 catalysts were also studied. The synergistic effect of active metals with suitable multi-metal modification could also improve the catalytic performance. Liu et al.[15] first prepared Cu-SSZ-13 catalysts by ion exchange and then used the impregnation method to introduce Mn and Ce metals into Cu-SSZ-13 to obtain Mn−Ce/Cu-SSZ-13 catalysts. Utilizing in situ IR and other characterization methods found that the synergistic interaction between Mn/Ce/Cu converted the bridged nitrate adsorbed on the catalyst surface into monodentate nitrate, which improved the performance of Cu-SSZ-13 catalysts at low temperatures.

The modifications of Cu-SSZ-13 by transition metals of Fe and Mn and lanthanide metals represented by Ce were widely studied. However, the modification of Cu-SSZ-13 by other transition metals was less studied. There were many studies related to the application of Zr in oxide catalysts. The introduction of Zr could improve the N_2 selectivity of catalysts.[16] The collaboration between Cu and other metals could enhance the catalyst structure stability,[17] improve the reduction performance, and strengthen the surface acid sites of the catalysts to enhance the NH_3-SCR activity.[18] Some researchers have also introduced Zr into zeolite catalysts. Peng et al. utilized different methods to introduce Zr into Cu-SSZ-13 catalysts (Cu-SSZ-13 was prepared using ion exchange). They found that the introduction of highly dispersed ZrO_2 could improve the high-temperature catalyst performance without having any effect on the low-temperature performance of the catalyst. The interaction between Zr and Cu could reduce the oxidation of NH_3.[19] Chen et al. introduced Zr and Fe into SSZ-13 zeolite using a one-pot method, and Zr/Fe-SSZ-13 catalysts with small amount of Zr doping were obtained. The introduction of Zr was found to improve the relative crystallinity of Fe-SSZ-13 catalysts, inhibit the migration and agglomeration of iron ions, and improve the hydrothermal stability of the catalysts.[20]

In this study, a small amount of Zr was introduced into the Cu-SSZ-13 catalyst obtained by ion exchange through the impregnation method. Zr-modified Cu-SSZ-13 catalysts with different Zr/Cu mass ratios were obtained. The NH_3-SCR performance was investigated. The catalysts were characterized by X-ray diffraction (XRD), ICP-OES, BET, X-ray photoelectron spectrometry (XPS), in situ diffuse reflectance infrared Fourier transform spectroscopy (DRIFTS), and so on to investigate the factors affecting the NH_3-SCR performance.

2. EXPERIMENT

2.1. Preparation of Cu-SSZ-13 and Zr-Modified Catalysts. A H-SSZ-13 molecular sieve with a Si/Al ratio of 6.5 was used, and the typical Cu loading mass fraction should be 2−3% for a low Si/Al ratio.[19] The Cu-SSZ-13 catalyst was prepared using the ion exchange method, and it was reported that the best balance of high-temperature durability and SCR activity could be achieved with a Cu loading mass fraction of about 2.2%.[19] The design target Cu loading mass fraction was 2.2%. Copper acetate monohydrate (Tianjin Beichen, AR) was used as the precursor. After a lot of experimental attempts and ICP-OES verification, the Cu-SSZ-13 catalyst with a Cu loading mass fraction of about 2.2% was obtained. The experiment was as follows: the copper acetate solution was prepared according to the calculation. The mass concentration of Cu^{2+} was 4.42 g/L, and the mass ratio of Cu^{2+} to molecular sieve was 4.5% which was put into the corresponding H-SSZ-13 molecular sieve, placed in a magnetic stirrer with heating and stirring at 73 ± 2 °C, and started for 4 h when the temperature reached 73 °C. Then, the catalyst was washed with deionized water after ion exchange, dried in an oven at 105 °C for 8 h, and calcined in a muffle furnace at 550 °C for 6 h after grinding. Under these conditions, we conducted several preparations of 30 g of samples, and the Cu content fluctuates between 2.179 and 2.246%. At last, the sample was ground again to obtain a Cu-SSZ-13 zeolite catalyst, marked as Cu−S. The Zr-modified Cu-SSZ-13 catalyst was prepared using the impregnation method. First, the pore volume of 1 g of Cu-SSZ-13 molecular sieve was titrated with deionized water to obtain the volume of water absorption. The Zr/Cu mass ratio of the modified catalyst was set to 0.1, 0.2, 0.4, 0.6, 0.8, and 1.0, respectively. The corresponding zirconium nitrate pentahydrate (Macklin, AR) solution was configured. Then, the solution was added dropwise to the samples while stirring. The samples were dried at 105 °C for 8 h in an oven. After that, the samples were calcined at a temperature of 550 °C for 6 h. The catalysts were ground to obtain Zr/Cu-SSZ-13 catalysts labeled as $Zr_{0.1}$Cu−S, $Zr_{0.2}$Cu−S, $Zr_{0.4}$Cu−S, $Zr_{0.6}$Cu−S, $Zr_{0.8}$Cu−S, and $Zr_{1.0}$Cu−S, respectively.

2.2. Catalyst Performance Measurement. Cu-SSZ-13 sample and modified Zr/Cu-SSZ-13 catalyst NH_3-SCR performance tests were carried out on a VDRT-200 SCR catalyst evaluation device; the inlet gas flow was composed of 0.1% NO, 0.1% NH_3, and 5% O_2 by volume fractions and N_2 as balance gas. The gas flow was dominated at 200 mL min^{-1} in the gas hourly space velocity (GHSV) of 24,000 h^{-1}, which was controlled using a mass flowmeter. 300 mg (about 0.5 mL) of the catalyst was added into the reactor. The catalyst efficiency was calculated using eq 1

$$\eta = \frac{[NO]_{in} - [NO_x]_{out}}{[NO]_{in}} \quad (1)$$

2.3. Catalyst Characterization. The XRD measurement in the 2θ range of 5−40° was performed on the DX-2700B X-ray diffractometer with Cu Kα radiation (λ = 0.15406 nm). The scanning speed was set to 2°/min, and the tube voltage and current were set to 50 kV and 30 mA, respectively.

The catalyst was tested by ICP-OES on a PerkinElmer Avio200 inductively coupled plasma optical emission spectrometer. 50 mg of the sample was dissolved in a mixed solution of hydrochloric acid and sulfuric acid, digested completely using a microwave digester and compared with the standard solution to obtain the actual metal content of the catalyst.

N_2 adsorption was carried out at 77 K using a V-Sorb 2800 automatic specific surface area analyzer to measure the BET surface areas, micropore diameters, and volumes (using single-point maximum adsorption and *t*-plot method).

NH_3 temperature-programed desorption (NH_3-TPD) and H_2-TPR were carried out on a Vodo-VDsorb-91i instrument. For the NH_3-TPD measurement, 0.05 g of the sample was pretreated at 500 °C under pure He gas flow of 30 mL min^{-1}

https://doi.org/10.1021/acsomega.2c05582
ACS Omega 2022, 7, 45144−45152

for 1 h to remove the impurities adsorbed on the sample surface. Then, it was cooled to 100 °C and saturated with 5% NH_3/N_2 gas for 45 min. After being purged by He gas flow (30 mL min^{-1}) for 1 h to remove the physically adsorbed NH_3, desorption of NH_3 was carried out from 100 to 700 °C at 10 °C min^{-1}. For the H_2-TPR measurement, 0.05 g of the sample was pretreated at 500 °C under pure He gas flow of 30 mL min^{-1} for 1 h to remove the impurities adsorbed on the sample surface, then cooled to 50 °C. Subsequently, the reduction process was performed from 50 to 900 °C at 10 °C min^{-1} in 10% H_2/Ar flow (10 mL min^{-1}).

The surface atomic concentration and element valence of catalysts were recorded using an X-ray photoelectron spectrometer (Thermo Escalab 250Xi) with Al Kα as the radiation source. Semi-quantitative analysis of the surface element content was obtained.

In situ DRIFTS was performed on a Shimadzu IRTracer-100 Fourier transform spectrometer with a spectra collection range of 4000−650 cm^{-1} and a resolution of 4 cm^{-1}. A mercury-cadmium-telluride detector was used for in situ cell IR detection (cooling by liquid nitrogen). The sample was mixed with KBr at a mass ratio of 1:50 and sent into the reactor, which was purged for 40 min at 400 °C under an Ar atmosphere. Subsequently, it was cooled to 150 °C to start the experiment. The gas flow was composed of 5% O_2, 1% NH_3, and 1% NO with Ar as the balance gas, and the total inlet gas flow was dominated at 100 mL min^{-1} using the flow controller.

3. RESULTS AND DISCUSSION

3.1. Catalytic Activity Measurements. The NO conversion of the synthesized Cu-SSZ-13 and Zr/Cu-SSZ-13 catalysts prepared in different Zr/Cu mass ratios is displayed in Figure 1. It showed that the Cu−S sample prepared using the ion-exchange method and Zr-modified catalysts using the impregnation method presented superior NH_3-SCR activity at a temperature range of 250−400 °C. The catalyst labeled as $Zr_{0.2}$Cu−S performed excellent NH_3-SCR at 200 °C with approximate 100% NO_x conversion efficiency. At a temperature of 450 °C, $Zr_{0.2}$Cu−S could also keep the NO conversion above 80%. The NO conversion efficiency of most of the catalysts decreased sharply when the temperature increased to 450 °C, which might be due to the oxidation of the NH_3 after the temperature reached 400 °C, leading to the decrease in NO_x conversion.[21] A moderate amount of Zr doping can improve the NO_x conversion of Cu-SSZ-13 catalysts, and Zr-doped-modified catalysts perform better NH_3-SCR activity than Cu-SSZ-13 at higher temperatures. However, an excessive Zr doping could also lead to a decrease in NO_x conversion at high temperatures. Compared with the origin Cu−S catalyst, the impregnated Zr-modified Cu−S catalyst with a Zr/Cu mass ratio of 0.2 improved low-temperature NO conversion performance and broadened the high-temperature reactive interval.

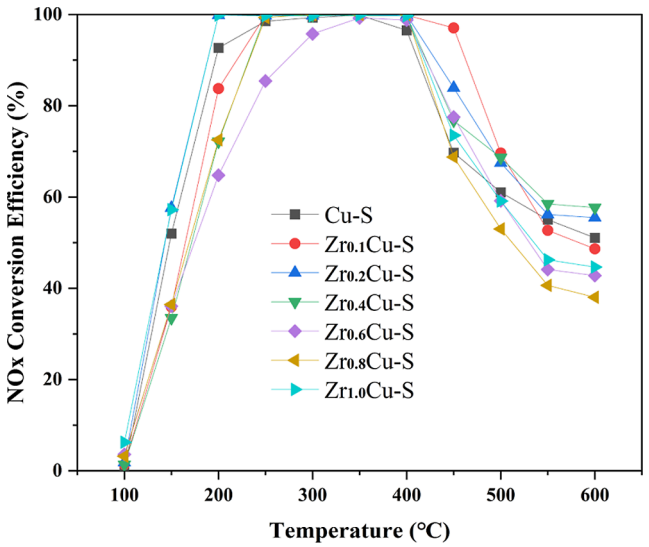

Figure 1. NO_x conversion performance of Cu−S and Zr/Cu−S with different Zr/Cu mass ratios.

3.2. XRD Test. In order to verify whether the lattice structure of the catalyst samples changed after Cu/Zr doping, XRD tests were carried out, and the results are shown in Figure 2. All samples showed distinctive peaks at 2θ = 9.56, 14.07, 16.11, 17.92, 20.74, 25.16, and 30.87°, which were consistent with the CHA structure peaks of SSZ-13 (2θ = 9.5, 14.0, 16.1, 17.8, 20.7, 25.0, and 30.7°).[22] It was indicated that the doping of Cu and Zr did not change the crystal structure of the molecular sieve significantly. The diffraction peak of 2θ = 9.5° presented a minor weakness with the increase in the metal loading, which might be due to the combination of metal ions with the zeolite framework, resulting in the deformation of the crystal octet ring and weakening of the planar (1 0 0) diffraction intensity.[23] The diffraction peaks of CuO (2θ = 35.60 and 38.80°) and Cu_2O (2θ = 36.44°) were not observed in the pattern, which indicated that Cu species were well dispersed in Cu−S and Zr-modified Cu−S catalysts.[24] M-ZrO_2 and t-ZrO_2 diffraction peaks of 2θ = 28.2 and 30.2°, respectively,[19] were not observed in the diffraction patterns, which indicated that the element of Zr may be uniformly dispersed as nanoparticles on the catalyst surface or present in the zeolite pores in the ionic form.

3.3. BET and ICP-OES Measurements. The parameters of the H-SSZ-13 molecular sieve and Cu−S and Zr-modified Cu−S catalysts with Cu and Zr element mass fraction, specific surface area, and pore structure are shown in Table 1.

A larger specific surface area of the catalyst could provide more active sites for the NH_3-SCR reaction,[25] which was beneficial to the NH_3-SCR reaction. After the Zr introduction, the specific surface area decreased significantly with the increase in the metal loading, which might be the increase in metal doping resulting in pore blockage. The larger the micropore volume and smaller the pore size, the more favorable the NH_3-SCR reaction was. $Zr_{0.2}$Cu−S demonstrated a larger pore volume and smaller pore size, which was one of the reasons for its superior NO_x conversion efficiency. Abnormal data of $Zr_{0.6}$Cu−S might be the corrosion of micropores during metal modification.

ICP-OES analysis showed that all the samples had a stable Cu loading of about 2.2%, which was consistent with the experimental design goals. However, the XRD pattern did not show the diffraction peaks of introduced metal, it also confirmed that the introduced metal elements were present in the pore channels in the ionic form or uniformly dispersed on the catalyst surface in the form of nanoparticles, which facilitated the NH_3-SCR reaction.

3.4. NH_3-TPD Measurement. The NH_3-TPD measurement was conducted to probe the acidity of Cu−S and Zr-modified catalysts, and the results are shown in Figure 3. All the catalysts exhibited three distinct NH_3 desorption peaks (A,

https://doi.org/10.1021/acsomega.2c05582
ACS Omega 2022, 7, 45144−45152

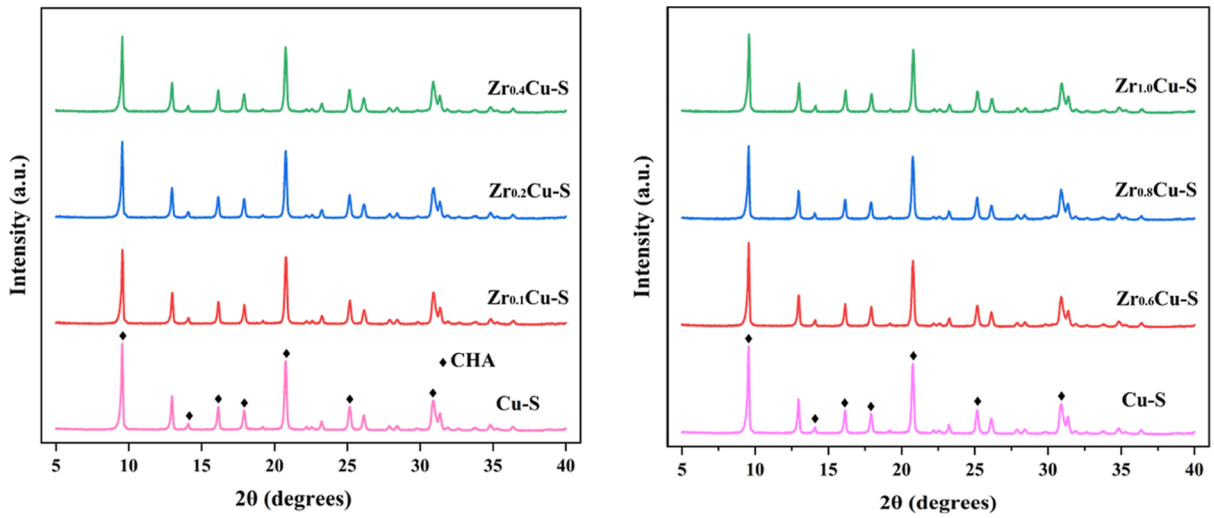

Figure 2. XRD patterns of the catalyst.

Table 1. BET and ICP-OES Results of Catalysts

sample	S_{BET}(m^2 g^{-1})[a]	V_{micro}(cm^3 g^{-1})[b]	V_{pore}(cm^3 g^{-1})[c]	D_{pore} (nm)[d]	Cu (wt %)	Zr (wt %)
H-SSZ-13	752.22	0.279	0.322	1.7115	—	—
Cu−S	720.56	0.264	0.299	1.6577	2.24	—
$Zr_{0.1}$Cu−S	695.11	0.253	0.288	1.7759	2.20	0.28
$Zr_{0.2}$Cu−S	704.52	0.262	0.286	1.6221	2.15	0.50
$Zr_{0.4}$Cu−S	647.52	0.265	0.298	1.8974	2.11	0.99
$Zr_{0.6}$Cu−S	628.70	0.217	0.443	2.9466	2.32	1.53
$Zr_{0.8}$Cu−S	594.83	0.256	0.283	1.6275	2.21	1.80
$Zr_{1.0}$Cu−S	519.77	0.191	0.223	1.7128	2.26	2.33

[a]Multi-point BET specific surface area. [b]*t*-Plot method microporous volume. [c]Highest single-point adsorption total pore volume. [d]$D = 4V/A$ by BET.

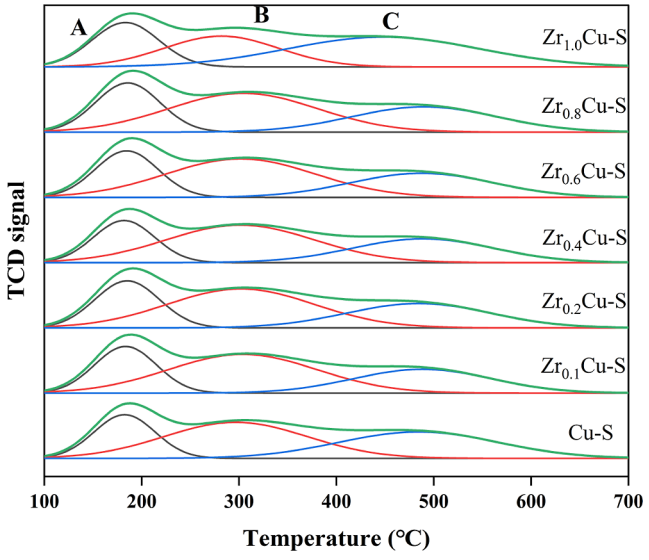

Figure 3. NH_3-TPD profiles for Cu−S and Zr-modified catalysts.

B, and C). The peak located near 185 °C could be attributed to the desorption of NH_3 adsorbed at weak Lewis acid sites;[26,27] the B peak appeared at ∼300 °C and could be assigned to the desorption of NH_3 from Cu^{2+} and strong Lewis acid sites; and the desorption peak C near 481 °C should be the desorption of NH_3 adsorbed at Brønsted acid sites.[27,28] The fitted profile was integrated and calculated to obtain the total NH_3 desorption. We found that $Zr_{0.8}$Cu−S had the largest integral area among all catalysts, followed by $Zr_{0.2}$Cu−S. Compared with the Cu−S sample, the integral area of the A and B peaks (Lewis acid sites) of $Zr_{0.2}$Cu−S was increased by 7%. Zr modification enhanced the NH_3 adsorption capacity. Lewis acid sites played an important role in the NH_3-SCR reaction at low temperatures, and we speculated that the rich Lewis acid site was one of the reasons for the excellent NH_3-SCR performance of $Zr_{0.2}$Cu−S at low temperatures.

3.5. H_2-TPR Measurement. Figure 4 shows the H_2-TPR results of Cu−S and Zr/Cu-SSZ-13 catalysts. All the lines demonstrated four reduction peaks. Generally, the reduction of Cu^{2+} has two steps: in the first, Cu^{2+} is reduced to Cu^+, and then, Cu^+ is reduced to Cu^0. Among them, peak A was located near 250 °C, which could be attributed to the reduction of Cu^{2+} to Cu^+ in the 8MRs cage and cage and D6Rs; the reduction peak near 385 °C should be the reduction of Cu_xO to Cu^0; and the reduction peaks of Cu species at temperatures higher than 500 °C are generally $Cu^+ \rightarrow Cu^0$; therefore, peaks C and D should be classified as the reduction of Cu^+ to Cu^0.[28−30] With the increase in the Zr loading, the moving forward peak C could be clearly observed in the spectra. Pure ZrO_2 is reduced around 421−425 °C. Therefore, we believed that this might be due to the reduction of Zr species of the catalyst.[19] The Cu^{2+} reduction peak of Cu−S at low temperatures (∼250 °C) was not obvious; however, the reduction peak of Cu^{2+} near 250 °C was significantly enhanced by the introduction of Zr. This might be because the Zr species promoted the Cu^{2+} reduction within the 8MRs cage and D6Rs, which improved the redox ability of the Cu active center; this

https://doi.org/10.1021/acsomega.2c05582
ACS Omega 2022, 7, 45144−45152

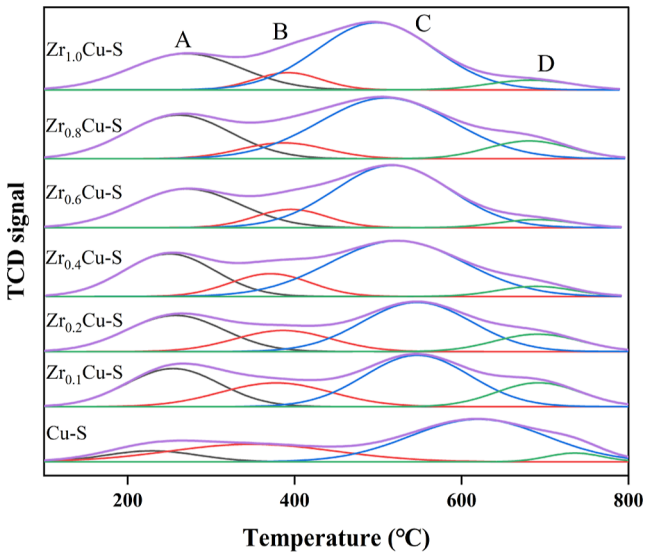

Figure 4. H_2-TPR profiles for Cu−S and Zr-modified catalysts.

change was beneficial to the NH_3-SCR reaction at low temperatures.

3.6. Copper and Zirconium Species. The XPS measurement was carried out to assess the effect of the Zr doping on the valence and surface content of Cu species. XPS profiles of Cu−S and $Zr_{0.2}Cu-S$ are shown in Figure 5. The valence state and content of Cu species present could be determined by the magnitude of the Cu 2p binding energy.

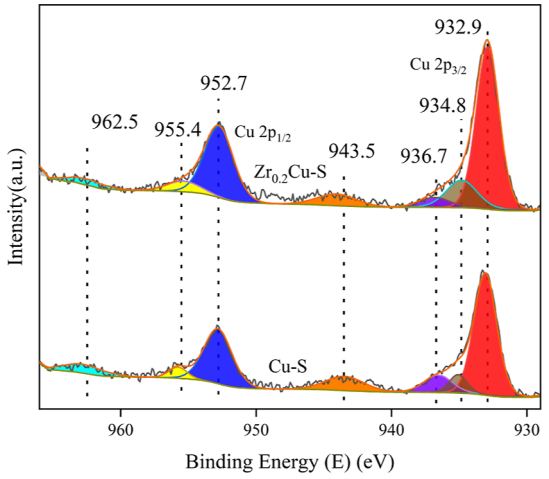

Figure 5. Cu 2p XPS profiles of different catalysts.

Under X-rays, the inner and valence electrons of the Cu element were excited, and the 2p shell energy level of Cu was divided into $2p_{3/2}$ and $2p_{1/2}$. The peaks of Cu $2p_{3/2}$ and Cu $2p_{1/2}$ appeared near the binding energy of 933 eV and 952.7 eV, respectively. The binding energy of 932.9 eV located near 933 eV and the main peak near 952.7 eV could be assigned to Cu^+.[31,32] The satellite peaks with binding energies of 934.8 and 936.7 eV appeared near the main peak at 932.9 eV, which could be ascribed to Cu^{2+} (Cu−O−Si−O) coordinated with oxygen in the zeolite framework and octahedrally coordinated Cu^{2+}, respectively.[10,29] The shake-up peak near 943.5 eV could be assigned to the presence of Cu^{2+}.[33] The low peak at 955.4 eV was the accompanying peak at 952.7 eV and the shake-up satellite peak at 962.5 eV could be classified as Cu^{2+}.[34] It could be seen from the profile that the doping of Zr changed the distribution of Cu active species on the catalyst surface, and an increase in the Cu^+ and Cu^{2+} peak integral area could be observed. XPS results showed that the Cu content on the sample surface increased from 2.7 to 2.89%. The migration of Cu active sites to the catalyst surface was beneficial to the surface SCR reaction. The integration of each peak area was calculated to obtain the content of each Cu species on the catalyst sample surface, as shown in Figure 6.

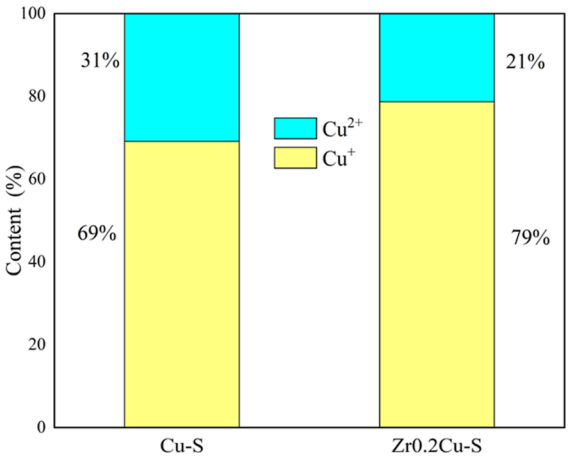

Figure 6. Change of Cu^+ and Cu^{2+} content on the catalyst surface.

The XPS profiles of Figure 7 showed the peaks of $3d_{3/2}$ and $3d_{5/2}$ of the Zr element at 184.6 and 182.2 eV, respectively.

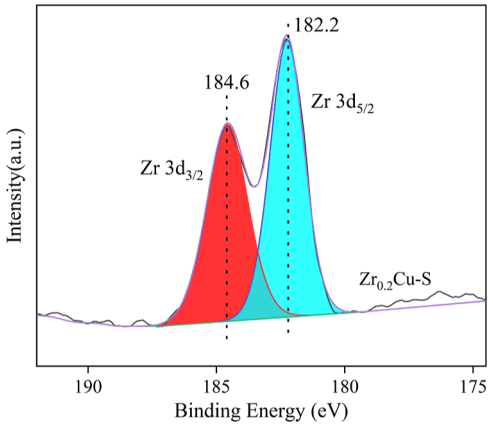

Figure 7. Zr 3d XPS profiles of $Zr_{0.2}Cu-S$.

The charge transfer between Cu and Zr on the surface of the zeolite leads to the higher binding energy of Zr $3d_{5/2}$ in the catalyst than that of metallic Zr (180.0 eV). The element Zr was present as Zr^{4+} on the surface of the molecular sieve.[35,36] The Zr doping could regulate the valence state of Cu elements on the catalyst surface, with a 10% increase in Cu^+ and a 10% decrease in Cu^{2+}. The redox interaction between Cu^+ and Cu^{2+} was crucial in the SCR reaction. According to the report,[34] simulations showed that O_2 adsorbs on Cu^+ to form Cu^+-O_2/H^+ species. Cu^+-O_2/H^+ could provide a reaction site for NO oxidation to NO_2 and react spontaneously with gas-phase NO to form Cu^{2+}−OH−NO_2, followed by NO_2 release to form Cu^{2+}−OH. Abundant Cu^+ played an important role in

https://doi.org/10.1021/acsomega.2c05582
ACS Omega 2022, 7, 45144−45152

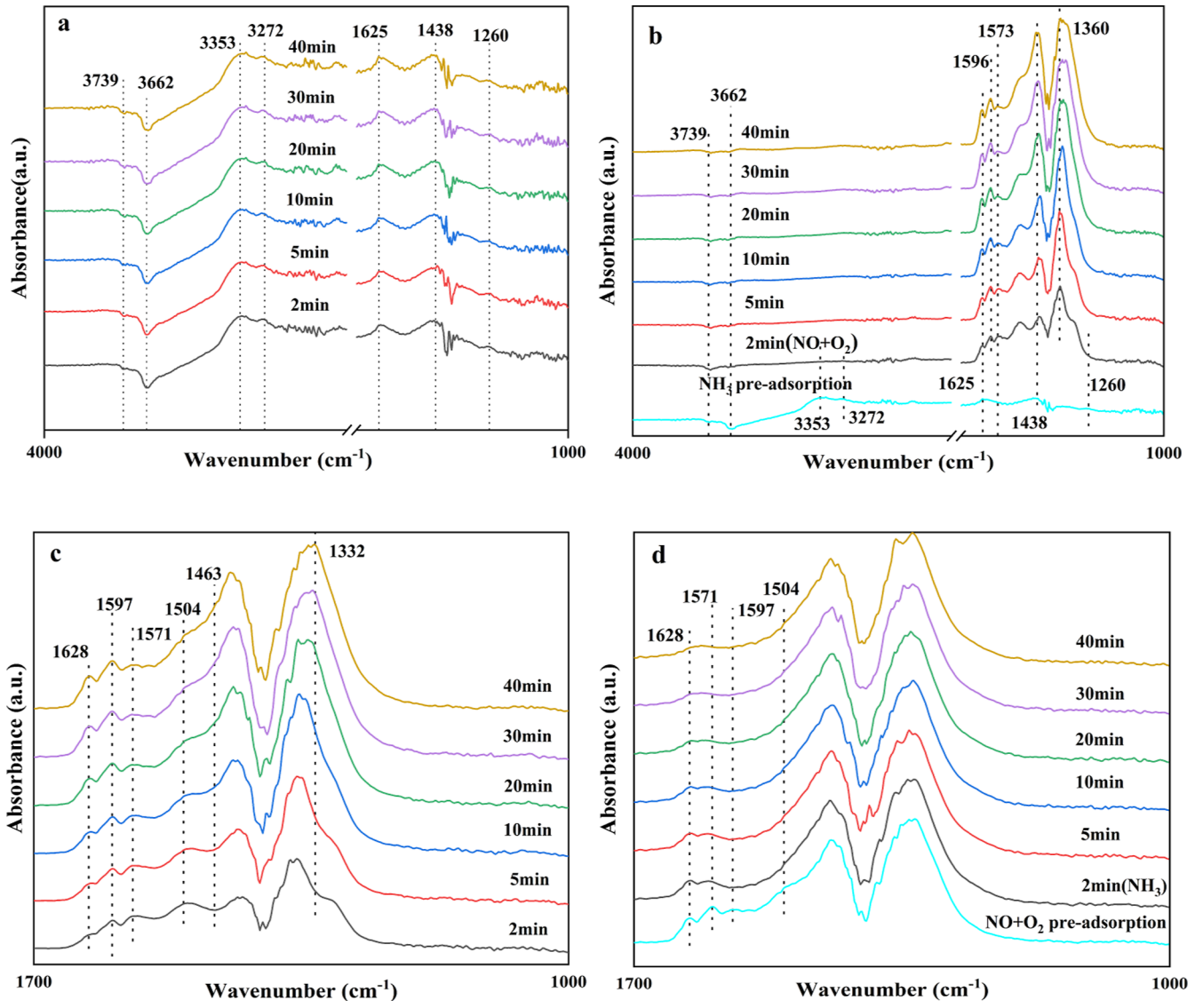

Figure 8. In situ DRIFTS spectra of the $Zr_{0.2}Cu-S$. (a) NH_3 adsorbed at 150 °C; (b) NO + O_2 reacted with pre-adsorbed NH_3 species at 150 °C; (c) NO + O_2 adsorption at 150 °C; and (d) NH_3 reacted with pre-adsorbed NO + O_2 at 150 °C.

promoting the fast SCR reaction by regulating the NO and NO_2 ratio of the SCR reaction. Generally, the fast-SCR reaction mainly occurred at low temperatures,[34,37,38] and the NH_3-SCR activity experimental results also showed that the doping of a moderate amount of Zr could enhance the NO conversion efficiency at low temperatures.

3.7. In Situ DRIFTS Study at Low Temperatures. *3.7.1. NH_3 Adsorption Experiment.* The acid sites on the surface of the $Zr_{0.2}Cu-S$ catalyst could be characterized by in situ DRIFTS NH_3 adsorption experiments, and the sample pretreatment method is described in Section 2.3. After pretreatment, the samples were cooled to 150 °C for background scanning, and then, the NH_3 gas flow with Ar as balance gas was adjusted to 100 mL min^{-1}. The NH_3 adsorption spectra of $Zr_{0.2}Cu-S$ at 2, 5, 10, 20, 30, and 40 min are shown in Figure 8a.

Generally, IR adsorption features of high wavenumber (>3000 cm^{-1}) were N−H stretching vibrations, and the low wavenumber features (<1700 cm^{-1}) were from N−H bending vibrations.[39] The spectra showed the adsorption peaks at 3353, 3272, 1625, 1438, and 1260 cm^{-1}. According to previous reports, bands at 3353, 1625, and 1260 cm^{-1} could be assigned to N−H stretching and bending vibrations of adsorbed NH_3 on Lewis acid sites. The bands at 3272 and 1438 cm^{-1} were from Al−O−NH^{4+} stretching and bending vibrations of NH_3 adsorption on the Brønsted acid sites.[39−43] Negative peaks could be observed at the bands of 3739 and 3662 cm^{-1}. The former could be attributed to the depletion of OH of surface terminal Si−OH groups, and the latter was from NH_3 adsorption onto bridging hydroxyl groups.[39,44] The presence of Brønsted acid sites and abundant Lewis acid sites on the catalyst surface was beneficial to the adsorption of NH_3.[45] While the Brønsted acid sites mainly played an important role in the SCR reaction at high temperatures and the Lewis acid sites facilitated the SCR reaction at low temperatures, the catalyst showed superior NH_3-SCR activity at low temperatures.

3.7.2. Reaction between NO + O_2 and Pre-adsorbed of NH_3 at Low Temperatures. In order to understand the reaction between NO + O_2 and pre-adsorbed NH_3, and the possible reaction paths, after the saturation of NH_3 adsorption, a 15 min Ar purge was carried out to remove extra NH_3 in

https://doi.org/10.1021/acsomega.2c05582
ACS Omega 2022, 7, 45144−45152

tubes and the reactor. After that, the gas flow was changed to NO + O_2 with Ar as the balance gas. Infrared signals were collected at 2, 5, 10, 20, 30, and 40 min, and the spectra of the reaction between NO + O_2 and pre-adsorbed NH_3 are shown in Figure 8b.

The spectra did not show a downtrend of NH_3 adsorption peaks, probably due to the reaction between adsorbed NH_3 species and NO + O_2 being too fast to observe at 150 °C (the signals collected after 2 min), which could also suggest the excellent NO conversion efficiency of the catalyst at low temperatures. The recovery of surface hydroxyl (Si−OH) and bridging hydroxyl (Al−OH−Si) species located at the bands of 3662 and 3739 cm^{-1} could be observed in the spectra, indicating that NH_3 at the sites was desorbed by Ar purging or adsorbed NH_3 species had been involved in the reaction.[39,44] The bands at 1573, 1596, and 1625 cm^{-1} can be attributed to the formation of nitrate species with different coordination.[46] The increasing peak at 1625 cm^{-1} should be assigned to nitrate adsorbed on metal ion exchange zeolites, and bridged nitrate also appears near this wavenumber.[43,45,47] The increasing band of 1360 cm^{-1} with time was attributed to the generation of monodentate nitrate species. In summary, at a low temperature of 150 °C, coordinated NH_3 could participate in the SCR reaction with gaseous NO + O_2, and the reaction follows the E−R mechanism.

3.7.3. NO + O_2 Adsorption Experiments. The sample pretreatment method is described in Section 2.3. After pretreatment, the sample was cooled to 150 °C for background scanning, and then, the NO + O_2 gas flow with Ar as the balance gas was adjusted to 100 mL min^{-1}. The NO + O_2 adsorption spectra of $Zr_{0.2}Cu−S$ at 2, 5, 10, 20, 30, and 40 min are shown in Figure 8c.

The increasing peak signal range of 1500−1300 cm^{-1} was from nitrate species (asymmetric stretching vibration of NO), which were considered to be nitrate species from the NO_x adsorbed onto metal sites.[46] The bands at 1628, 1597, 1571, and 1504 cm^{-1} were attributed to adsorbed NO_2 (Cu−NO_2), bridged nitrate, bidentate nitrate, and monodentate nitrate species, respectively.[43,47−49] This demonstrated that NO could be converted to NO_2 and adsorbed on the catalyst surface under aerobic conditions at 150 °C. The adsorption state approached saturated after 10 min, indicating that the catalyst had a strong adsorption capacity for NO_x.

3.7.4. Reaction between NH_3 and Pre-adsorbed of NO + O_2 at Low Temperatures. In order to understand the reaction between NH_3 and pre-adsorbed NO + O_2, and the possible reaction paths, after the saturation of NO + O_2 adsorption, a 15 min Ar purge was carried out to remove extra NO + O_2 in tubes and the reactor. After that, the gas flow was changed to NH_3 with Ar as the balance gas. Infrared signals were collected at 2, 5, 10, 20, 30, and 40 min, and the spectra of reaction between NO + O_2 and pre-adsorbed NH_3 are shown in Figure 8d.

NH_3 could be adsorbed at 1260 and 1438 cm^{-1}, but no clear peaks were observed in the spectra. There was a visible decreasing trend of adsorbed NO_2 and bridged nitrate species at the bands of 1628 and 1597 cm^{-1} at a low temperature of 150 °C, indicating that the adsorbed NO_2 (Cu−NO_2) and bridged nitrate Cu−O_2−NO− species reacted with coordinated NH_3 and the reaction following the L−H mechanism. No obvious change was observed at the bands of 1571 and 1504 cm^{-1}. However, compared with the pre-adsorbed NO + O_2 spectra, it was found that the original nitrate species on the site were consumed. We considered that the reaction rate was too fast to be observed, where the bidentate nitrate and monodentate nitrate species were already consumed by gaseous NH_3 within 2 min. This also could verify the excellent NO conversion efficiency of the catalyst at low temperatures. In conclusion, the SCR reaction of the catalyst at a low temperature of 150 °C followed both L−H and E−R mechanisms, and the abundant adsorption sites and superior low-temperature activity promoted the SCR reaction at low temperatures.

4. CONCLUSIONS

Cu-SSZ-13 was prepared using the ion-exchange method, and Zr was introduced into Cu-SSZ-13 using the impregnation method to obtain Zr-modified Cu-SSZ-13 catalysts with different Zr contents.

(1) Among a series of catalysts, $Zr_{0.2}Cu−S$ significantly broadened the active temperature range of the Cu-SSZ-13 catalyst, with NO conversion efficiency close to 100% in the temperature range of 200−400 °C and still over 80% at 450 °C.

(2) Cu and Zr elements could be well dispersed on the catalyst surface, and the structure of the zeolite was not destroyed, with a decrease in specific surface area.

(3) The doping of Zr improved the distribution of Cu species on the catalyst surface, and the interaction between Zr and Cu could regulate the proportion of Cu^{2+} and Cu^{+} on the zeolite surface to increase the Cu^{+}. Abundant Cu^{+} could provide the conditions for fast SCR reaction at low temperatures. H_2-TPR also showed that the catalyst demonstrated excellent reduction performance at low temperatures.

(4) NH_3-TPD and in situ DRIFTS studies showed that there were Brønsted acid sites and abundant Lewis acid sites on the surface of $Zr_{0.2}Cu−S$, which could provide more adsorption sites for NH_3. The Lewis acid sites were beneficial to the SCR reaction at low temperatures, and the catalyst also showed excellent NO conversion efficiency at low temperatures.

(5) The transient reactions between NH_3 and NO + O_2 showed that the SCR reactions occurring on the catalyst surface at a low temperature of 150 °C follow both L−H and E−R mechanisms, which were also vital for the superior low-temperature activity of the catalyst.

AUTHOR INFORMATION

Corresponding Author

Shuo Yang − *Vehicle & Transportation Engineering Institute, Henan University of Science and Technology, Luoyang 471003, China;* orcid.org/0000-0001-9261-1973; Email: yangs98966@163.com

Authors

Huiyong Du − *Vehicle & Transportation Engineering Institute, Henan University of Science and Technology, Luoyang 471003, China*

Ke Li − *Gu an Denox Environment&Technology Holdings Co., Ltd., Beijing 065000, China*

Qian Shen − *Gu an Denox Environment&Technology Holdings Co., Ltd., Beijing 065000, China*

https://doi.org/10.1021/acsomega.2c05582
ACS Omega 2022, 7, 45144−45152

Min Li − *Vehicle & Transportation Engineering Institute, Henan University of Science and Technology, Luoyang 471003, China*

Xuetao Wang − *Vehicle & Transportation Engineering Institute, Henan University of Science and Technology, Luoyang 471003, China*

Chenyang Fan − *Vehicle & Transportation Engineering Institute, Henan University of Science and Technology, Luoyang 471003, China;* orcid.org/0000-0001-5684-2547

Complete contact information is available at: https://pubs.acs.org/10.1021/acsomega.2c05582

Notes

The authors declare no competing financial interest.

Credit authorship contribution statement: **Huiyong Du:** ideas, supervision, and validation. **Shuo Yang:** experiment, data curation, and writing original draft. **Ke Li** and **Qian Shen:** experiment equipment and experimental guidance. **Min Li:** validation. **Xuetao Wang:** experimental guidance and validation. **Chenyang Fan:** validation and funding acquisition.

■ ACKNOWLEDGMENTS

This work is financially supported by the National Natural Science Foundation of China (no. 52006054) and the Bilingual teaching project of Henan University of Science and Technology (Emissions from Internal Combustion Engine).

■ REFERENCES

(1) Wang, Y.; Li, Z.; Fan, R.; Guo, X.; Zhang, C.; Wang, Y.; Ding, Z.; Wang, R.; Liu, W. Deactivation and Regeneration for the SO_2-Poisoning of a Cu-SSZ-13 Catalyst in the NH_3-SCR Reaction. *Catalysts* **2019**, *9*, 797.

(2) Ladshaw, A.; Pihl, J. Measurement and Modeling of the effects of exhaust composition and hydrothermal aging on the ammonia storage capacity of a commercial Cu-SSZ-13 catalyst. *Appl. Catal., B* **2022**, *303*, 120898.

(3) González, J. M.; Villa, A. L. High Temperature SCR Over Cu-SSZ-13 and Cu-SSZ-13+ Fe-SSZ-13: Activity of Cu^{2+} and $[CuOH]^{1+}$ Sites and the Apparent Promoting Effect of Adding Fe into Cu-SSZ-13 Catalyst. *Catal. Lett.* **2021**, *151*, 3011−3019.

(4) Gao, F.; Szanyi, J. On the hydrothermal stability of Cu/SSZ-13 SCR catalysts. *Appl. Catal., A* **2018**, *560*, 185−194.

(5) Gao, F.; Kollár, M.; Kukkadapu, R. K.; Washton, N. M.; Wang, Y.; Szanyi, J.; Peden, C. H. Fe/SSZ-13 as an NH3-SCR catalyst: A reaction kinetics and FTIR/Mössbauer spectroscopic study. *Appl. Catal., B* **2015**, *164*, 407−419.

(6) Fickel, D. W.; D'Addio, E.; Lauterbach, J. A.; Lobo, R. F. The ammonia selective catalytic reduction activity of copper-exchanged small-pore zeolites. *Appl. Catal., B* **2011**, *102*, 441−448.

(7) Fahami, A.; Günter, T.; Doronkin, D.; Casapu, M.; Zengel, D.; Vuong, T.; Simon, M.; Breher, F.; Kucherov, A.; Brückner, A.; Grunwaldt, J.-D. The dynamic nature of Cu sites in Cu-SSZ-13 and the origin of the seagull NOx conversion profile during NH_3-SCR. *React. Chem. Eng.* **2019**, *4*, 1000−1018.

(8) Shishkin, A.; Kannisto, H.; Carlsson, P.-A.; Härelind, H.; Skoglundh, M. Synthesis and functionalization of SSZ-13 as an NH_3-SCR catalyst. *Catal. Sci. Technol.* **2014**, *4*, 3917−3926.

(9) Gao, F.; Wang, Y.; Kollár, M.; Washton, N. M.; Szanyi, J.; Peden, C. H. A comparative kinetics study between Cu/SSZ-13 and Fe/SSZ-13 SCR catalysts. *Catal. Today* **2015**, *258*, 347−358.

(10) Zhang, R.; Li, Y.; Zhen, T. Ammonia selective catalytic reduction of NO over Fe/Cu-SSZ-13. *RSC Adv.* **2014**, *4*, 52130−52139.

(11) Wang, Y.; Xie, L.; Liu, F.; Ruan, W. Effect of preparation methods on the performance of CuFe-SSZ-13 catalysts for selective catalytic reduction of NOx with NH_3. *J. Environ. Sci.* **2019**, *81*, 195−204.

(12) Usui, T.; Liu, Z.; Ibe, S.; Zhu, J.; Anand, C.; Igarashi, H.; Onaya, N.; Sasaki, Y.; Shiramata, Y.; Kusamoto, T.; Wakihara, T. Improve the hydrothermal stability of Cu-SSZ-13 zeolite catalyst by loading a small amount of Ce. *ACS Catal.* **2018**, *8*, 9165−9173.

(13) Deng, D.; Deng, S.; He, D.; Wang, Z.; Chen, Z.; Ji, Y.; Yan, G.; Hou, G.; Liu, L.; He, H. A comparative study of hydrothermal aging effect on cerium and lanthanum doped Cu/SSZ-13 catalysts for NH_3-SCR. *J. Rare Earths* **2021**, *39*, 969−978.

(14) Li, X.; Feng, J.; Xu, Z.; Wang, J.; Wang, Y.; Zhao, W. Cerium modification for improving the performance of Cu-SSZ-13 in selective catalytic reduction of NO by NH_3. *React. Kinet., Mech. Catal.* **2019**, *128*, 163−174.

(15) Liu, Q.; Fu, Z.; Ma, L.; Niu, H.; Liu, C.; Li, J.; Zhang, Z. MnOx-CeO_2 supported on Cu-SSZ-13: A novel SCR catalyst in a wide temperature range. *Appl. Catal., A* **2017**, *547*, 146−154.

(16) Sun, C.; Liu, H.; Chen, W.; Chen, D.; Yu, S.; Liu, A.; Dong, L.; Feng, S. Insights into the Sm/Zr co-doping effects on N_2 selectivity and SO_2 resistance of a MnOx-TiO_2 catalyst for the NH_3-SCR reaction. *Chem. Eng. J.* **2018**, *347*, 27−40.

(17) Chen, L.; Ren, S.; Liu, W.; Yang, J.; Chen, Z.; Wang, M.; Liu, Q. Low-temperature NH_3-SCR activity of M (M= Zr, Ni and Co) doped MnOx supported biochar catalysts. *J. Environ. Chem. Eng.* **2021**, *9*, 106504.

(18) Shen, B.; Wang, Y.; Wang, F.; Liu, T. The effect of Ce−Zr on NH_3-SCR activity over $MnO_{x\ (0.6)}/Ce_{0.5}Zr_{0.5}O_2$ at low temperature. *Chem. Eng. J.* **2014**, *236*, 171−180.

(19) Peng, B.; Rappé, K. G.; Cui, Y.; Gao, F.; Szanyi, J.; Olszta, M. J.; Walter, E. D.; Wang, Y.; Holladay, J. D.; Goffe, R. A. Enhancement of high-temperature selectivity on Cu-SSZ-13 towards NH_3-SCR reaction from highly dispersed ZrO_2. *Appl. Catal., B* **2020**, *263*, 118359.

(20) Chen, Z.; Liu, Q.; Guo, L.; Zhang, S.; Pang, L.; Guo, Y.; Li, T. The promoting mechanism of in situ Zr doping on the hydrothermal stability of Fe-SSZ-13 catalyst for NH_3-SCR reaction. *Appl. Catal., B* **2021**, *286*, 119816.

(21) Zhao, Z.; Yu, R.; Zhao, R.; Shi, C.; Gies, H.; Xiao, F.-S.; De Vos, D.; Yokoi, T.; Bao, X.; Kolb, U.; Feyen, M.; McGuire, R.; Maurer, S.; Moini, A.; Müller, U.; Zhang, W. Cu-exchanged Al-rich SSZ-13 zeolite from organotemplate-free synthesis as NH_3-SCR catalyst: Effects of Na^+ ions on the activity and hydrothermal stability. *Appl. Catal., B* **2017**, *217*, 421−428.

(22) Wang, J.; Shao, L.; Wang, C.; Wang, J.; Shen, M.; Li, W. Controllable preparation of various crystal size and nature of intra-crystalline diffusion in Cu/SSZ-13 NH_3-SCR catalysts. *J. Catal.* **2018**, *367*, 221−228.

(23) Zhang, T.; Qiu, F.; Chang, H.; Li, X.; Li, J. Identification of active sites and reaction mechanism on low-temperature SCR activity over Cu-SSZ-13 catalysts prepared by different methods. *Catal. Sci. Technol.* **2016**, *6*, 6294−6304.

(24) Xie, L.; Liu, F.; Ren, L.; Shi, X.; Xiao, F.-S.; He, H. Excellent performance of one-pot synthesized Cu-SSZ-13 catalyst for the selective catalytic reduction of NOx with NH_3. *Environ. Sci. Technol.* **2014**, *48*, 566−572.

(25) Guo, D.; Guo, R.; Duan, C.; Liu, Y.; Wu, G.; Qin, Y.; Pan, W. The enhanced K resistance of Cu-SSZ-13 catalyst for NH_3-SCR reaction by the modification with Ce. *Mol. Catal.* **2021**, *502*, 111392.

(26) Wang, M.; Peng, Z.; Zhang, C.; Liu, M.; Han, L.; Hou, Y.; Huang, Z.; Wang, J.; Bao, W.; Chang, L. Effect of Copper Precursors on the Activity and Hydrothermal Stability of Cu^{II}-SSZ-13 NH_3-SCR Catalysts. *Catalysts* **2019**, *9*, 781.

(27) Tian, H.; Ping, Y.; Zhang, Y.; Zhang, Z.; Sun, L.; Liu, P.; Zhu, J.; Yang, X. Atomic layer deposition of silica to improve the high-temperature hydrothermal stability of Cu-SSZ-13 for NH_3-SCR of NOx. *J. Hazard. Mater.* **2021**, *416*, 126194.

(28) Zhang, S.; Ming, S.; Guo, L.; Bian, C.; Meng, Y.; Liu, Q.; Dong, Y.; Bi, J.; Li, D.; Wu, Q.; Qin, K.; Chen, Z.; Pang, L.; Cai, W.; Li, T. Controlled synthesis of Cu-based SAPO-18/34 intergrowth zeolites for selective catalytic reduction of NOx by ammonia. *J. Hazard. Mater.* **2021**, *414*, 125543.
(29) Liu, J.; Tang, X.; Xing, C.; Jin, T.; Yin, Y.; Wang, J. Niobium modification for improving the high-temperature performance of Cu-SSZ-13 in selective catalytic reduction of NO by NH_3. *J. Solid State Chem.* **2021**, *296*, 122028.
(30) Chen, Z.; Fan, C.; Pang, L.; Ming, S.; Guo, W.; Liu, P.; Chen, H.; Li, T. One-pot synthesis of high performance Cu-SAPO-18 catalyst for NO reduction by NH_3-SCR: Influence of silicon content on the catalytic properties of Cu-SAPO-18. *Chem. Eng. J.* **2018**, *348*, 608−617.
(31) Zhao, S.; Huang, L.; Jiang, B.; Cheng, M.; Zhang, J.; Hu, Y. Stability of Cu−Mn bimetal catalysts based on different zeolites for NOx removal from diesel engine exhaust. *Chin. J. Catal.* **2018**, *39*, 800−809.
(32) Wang, L.; Gaudet, J. R.; Li, W.; Weng, D. Migration of Cu species in Cu/SAPO-34 during hydrothermal aging. *J. Catal.* **2013**, *306*, 68−77.
(33) Ma, Y.; Li, Z.; Zhao, N.; Teng, Y. One-pot synthesis of Cu−Ce co-doped SAPO-5/34 hybrid crystal structure catalysts for NH_3-SCR reaction with SO_2 resistance. *J. Rare Earths* **2021**, *39*, 1217−1223.
(34) Li, Y.; Deng, J.; Song, W.; Liu, J.; Zhao, Z.; Gao, M.; Wei, Y.; Zhao, L. Nature of Cu species in Cu−SAPO-18 catalyst for NH_3−SCR: combination of experiments and DFT calculations. *J. Phys. Chem. C* **2016**, *120*, 14669−14680.
(35) Guo, M.; Liu, Q.; Liu, C.; Wang, X.; Bi, Y.; Fan, B.; Ma, D.; Liang, X.; Li, Z. Rational design of novel CrZrOx catalysts for efficient low temperature SCR of NOx. *Chem. Eng. J.* **2021**, *413*, 127554.
(36) Bin, F.; Song, C.; Lv, G.; Song, J.; Wu, S.; Li, X. Selective catalytic reduction of nitric oxide with ammonia over zirconium-doped copper/ZSM-5 catalysts. *Appl. Catal., B* **2014**, *150−151*, 532−543.
(37) Paolucci, C.; Verma, A. A.; Bates, S. A.; Kispersky, V. F.; Miller, J. T.; Gounder, R.; Delgass, W. N.; Ribeiro, F. H.; Schneider, W. F. Isolation of the Copper Redox Steps in the Standard Selective Catalytic Reduction on Cu-SSZ-13. *Angew. Chem., Int. Ed.* **2014**, *53*, 11828−11833.
(38) Li, W.-J.; Li, T.-Y.; Wey, M.-Y. Preferred enhancement of fast-SCR by Mn/CeSiOx catalyst: Study on Ce/Si promotion and shape dependence. *Chem. Eng. J.* **2021**, *403*, 126317.
(39) Wang, X.; Sun, Y.; Han, F.; Zhao, Y. Effect of Fe addition on the structure and SCR reactivity of one-pot synthesized Cu-SSZ-13. *J. Environ. Chem. Eng.* **2022**, *10*, 107888.
(40) Su, W.; Chang, H.; Peng, Y.; Zhang, C.; Li, J. Reaction pathway investigation on the selective catalytic reduction of NO with NH3 over Cu/SSZ-13 at low temperatures. *Environ. Sci. Technol.* **2015**, *49*, 467−473.
(41) Luo, J.; Wang, D.; Kumar, A.; Li, J.; Kamasamudram, K.; Currier, N.; Yezerets, A. Identification of two types of Cu sites in Cu/SSZ-13 and their unique responses to hydrothermal aging and sulfur poisoning. *Catal. Today* **2016**, *267*, 3−9.
(42) Li, R.; Wang, P.; Ma, S.; Yuan, F.; Li, Z.; Zhu, Y. Excellent selective catalytic reduction of NOx by NH_3 over Cu/SAPO-34 with hierarchical pore structure. *Chem. Eng. J.* **2020**, *379*, 122376.
(43) Fu, G.; Yang, R.; Liang, Y.; Yi, X.; Li, R.; Yan, N.; Zheng, A.; Yu, L.; Yang, X.; Jiang, J. Enhanced hydrothermal stability of Cu/SSZ-39 with increasing Cu contents, and the mechanism of selective catalytic reduction of NOx. *Microporous Mesoporous Mater.* **2021**, *320*, 111060.
(44) Liang, H.; Gui, K.; Zha, X. DRIFTS study of γ-Fe_2O_3 nano-catalyst for low-temperature selective catalytic reduction of NOx with NH_3. *Can. J. Chem. Eng.* **2016**, *94*, 1668−1675.
(45) Zhu, N.; Shan, Y.; Shan, W.; Sun, Y.; Liu, K.; Zhang, Y.; He, H. Distinct NO_2 Effects on Cu-SSZ-13 and Cu-SSZ-39 in the Selective Catalytic Reduction of NOx with NH_3. *Environ. Sci. Technol.* **2020**, *54*, 15499−15506.
(46) Huang, H. Y.; Yang, R. T. Removal of NO by Reversible Adsorption on Fe−Mn Based Transition Metal Oxides. *Langmuir* **2001**, *17*, 4997−5003.
(47) Wang, D.; Zhang, L.; Kamasamudram, K.; Epling, W. S. In situ DRIFTS study of selective catalytic reduction of NOx by NH_3 over Cu-exchanged SAPO-34. *ACS Catal.* **2013**, *3*, 871−881.
(48) Yao, X.; Zhang, L.; Li, L.; Liu, L.; Cao, Y.; Dong, X.; Gao, F.; Deng, Y.; Tang, C.; Chen, Z.; Dong, L.; Chen, Y. Investigation of the structure, acidity, and catalytic performance of $CuO/Ti_{0.95}Ce_{0.05}O_2$ catalyst for the selective catalytic reduction of NO by NH_3 at low temperature. *Appl. Catal., B* **2014**, *150−151*, 315−329.
(49) Wu, G.; Liu, S.; Chen, Z.; Yu, Q.; Chu, Y.; Xiao, H.; Peng, H.; Fang, D.; Deng, S.; Chen, Y. Promotion effect of alkaline leaching on the catalytic performance over Cu/Fe-SSZ-13 catalyst for selective catalytic reduction of NOx with NH_3. *J. Taiwan Inst. Chem. Eng.* **2022**, *134*, 104355.

https://doi.org/10.1021/acsomega.2c05582
ACS Omega 2022, 7, 45144−45152